

# 連続フレーム画像を用いた反射パラメータの推定法

張 曉華\* 中西 良成\* 小林 希一\* 三ッ峰 秀樹\*\* 齋藤 豪\*\*\*

\*NHK エンジニアリングサービス

\*\*NHK 放送技術研究所

\*\*\*東京工業大学精密工学研究所

## Estimation of Surface Reflectance Parameters from Image Sequences

Xiaohua Zhang\* Yoshinari Nakanishi\* Kiichi Kobayashi\*

Hideki Mitsumine\*\*

Suguru Saito\*\*\*

\*NHK Engineering Services Inc.

\*\*NHK Science and Technical Research Laboratories

\*\*\*Tokyo Institute of Technology

### Abstract

We have developed a technique for estimating the diffuse and specular reflectance parameters of a rotating 3D object from an image sequence taken by a high-definition TV camera with a fixed position and direction and with a fixed-direction light source. Many researchers have studied the computation of reflectance parameters from the separated diffuse and specular components. However, for a complicated texture, complete separation is difficult to achieve. Unlike other methods, our technique estimates diffuse and specular parameters directly from the raw RGB data by iteratively minimizing fitting errors without knowing the light source color and object color. The diffuse and specular components can then be separated using the estimated diffuse and specular reflectance parameters. Experimental results with both synthesized and real data demonstrate that this approach effectively and stably recovers the reflectance parameters.

### 1. Introduction

Object reflectance properties are important in the acquisition of object models and textures to generate highly realistic synthesized images in computer graphics applications such as virtual reality, virtual museums, and virtual studios. Early research emphasized color space analysis for image segmentation by partitioning a color histogram into clusters, and several papers have discussed use of the dichromatic reflectance model to describe the illumination of a uniformly colored object in the color space [1,2] to enable separation of the diffuse reflection and specular reflection components. The separated components are used to segment a color image without disturbing the image highlight [3]. However, since this method is based on the assumption that the object is uniformly colored, it cannot handle the reflectance from objects with complex textures.

The separation of reflection components by polarimetric imaging has recently drawn interest. Nayar, Fang and Boulton [4] introduced a technique to separate the reflection components of a reflectance object with a complex texture by using polarization. They achieved high quality separation by assuming that diffuse reflection tends to be unpolarized while preserving the polarization characteristics of the incident light. The dichromatic model was used to compute reflection components for each point.

Other techniques have been reported, such as shape from shading [5, 6] and photometric stereo [7,8] for analyzing images to recover the surface reflectance properties along with the surface shape under the assumption that the real object is Lambertian. Bernardini et al. [15] proposed constructing object models from range images by geometric alignment based on automatically

selected points and obtained a high quality texture covering the generated model from intensity images by using a unique weighting scheme. This approach can also be used to process occlusions by applying a depth map.

Recovering object reflectance properties from a color image sequence by using the concept of the temporal color space has been proposed [9] and successfully applied for object shape and reflectance modeling [10]. This method separates the diffuse and specular components and then computes the reflectance from the separated components using a known calibrated specular color vector and a measured diffuse reflection color.

Unlike the methods mentioned above, we estimate reflectance properties directly from a intensity image sequence to reduce the errors during separation. The computed diffuse and specular reflectance properties are then used to separate the two components. The reflectance properties are estimated by applying an iterative algorithm to fit the color values from different views to a nonlinear reflection model for each 3D point on the surface. This permits more effective and stable recovery because the fitting is based on the raw RGB data used to compute all model parameters.

This paper is organized as follows: Section 2 explains the experimental setup we used to obtain the color image sequence. Section 3 describes the reflection model and the iterative nonlinear fitting algorithm used to estimate reflectance properties and to separate the two reflection components. In Section 4 we discuss preliminary experimental results concerning diffuse and specular components separated using the computed reflectance properties, and in Section 5 we conclude and discuss our future work.

## 2. Experimental setup

The experimental setup of our image-acquisition system is illustrated in Fig. 1. The object whose reflectance properties were to be estimated was mounted on a rotary table whose rotation in the direction shown was controlled with a PC. The position and orientation of an HDTV camera relative to the rotary table were fixed. The point light source direction was also fixed, and was measured under the assumption that the distance

between the light source and object was greater than the object diameter. The color image sequences were obtained by rotating the 3D object around the rotation axis in fixed steps; for example, a step of 2 degrees would result in a sequence that contained 180 images. A single incandescent lamp was the light source and we measured the light source direction to compute reflectance properties and the surface normal.

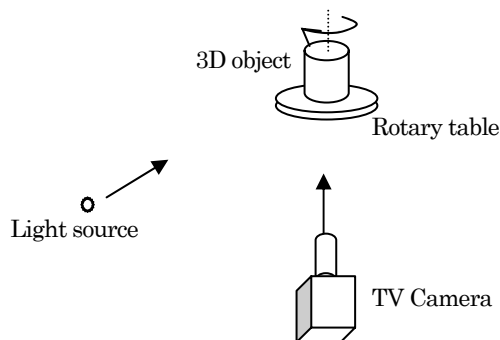


Figure 1. Experimental setup

To obtain the intensity variation of a 3D point on the surface, the camera parameters [11], rotation axis, and rotary table location were well calibrated. The 3D coordinates in a camera coordinate system for each point on the object's 3D surface were computed according to a modeling approach [14] and then reprojected onto each image to obtain the RGB values of the corresponding image pixels. In our experiments, the reprojected pixel was sampled as the average of a small window with a size such as  $3 \times 3$  pixels to reduce the random noise under the assumption that the intensity variation on the image was smooth.

## 3. Reflectance properties estimation

The reflection from a 3D point is related to the normal of this point, the light direction, and the viewing direction. The obtained reflection variation from all angles allows us to compute the reflectance properties. Once the RGB data for each point on the 3D object surface are obtained, the reflectance properties can be analyzed. We did this estimation for each pixel independently of the neighboring pixels.

### 3.1. Reflectance modeling

Figure 2 shows the geometry of our experimental setup. The optical axis of the camera was collinear

with the  $z$  axis and the rotation axis of the rotary table was collinear with the  $y$  axis. Vector  $n$  is the normal of a 3D point on the object surface and  $L$  is the unit direction vector of the point light source. Vectors  $L'$  and  $n'$  are projections of  $L$  and  $n$  onto the  $XOZ$  plane.  $\varphi_L$  is the angle between the light source direction and the  $y$  axis and  $\theta_L$  is the angle between the projection  $L'$  of  $L$  and the  $z$  axis. We used trigonometry to measure  $\varphi_L$  and  $\theta_L$  in advance.  $\varphi_n$  is the angle between the normal and the  $y$  axis;  $\theta_n$  is the angle between the projection  $n'$  of normal vector  $n$  and the  $x$  axis.

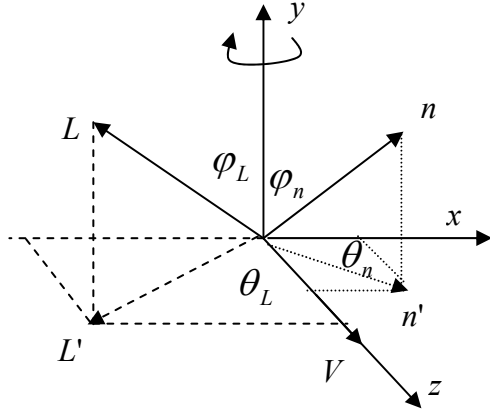


Figure 2. Geometry of experimental setup

Since the object surface reflectance can be modeled as a linear combination of the diffuse and specular reflection components for each channel, we used a simplified Torrance-Sparrow model [12] to describe this combination in the equation:

$$I = I_d + I_s = K_d(L \cdot n) + K_s e^{-\alpha^2/2\sigma^2}, \quad (1)$$

where  $L \cdot n$  is the inner product of two vectors,  $K_d$  is the diffuse reflection parameter and  $K_s$  is the specular reflection parameter. Parameter  $\alpha$  is the angle between the surface normal and the bisector of the light source direction and view direction.  $\sigma$  is the standard deviation of a facet slope in the Torrance-Sparrow model.

When coordinates  $(\varphi_L, \theta_L)$  are used to express the light direction and  $(\varphi_n, \theta_n + \theta)$  are used to express the normal after  $\theta$  angle rotation,

according to Eq. (1) after some mathematical rearrangement, the diffuse component can be written as:

$$I_d = A \sin \theta + B \cos \theta + C, \quad (2)$$

where parameters  $A$ ,  $B$  and  $C$  in Eq. (2) are defined as:

$$\begin{cases} A = K_d t_1 \sin \varphi_n \\ B = K_d t_2 \sin \varphi_n \\ C = K_d t_c \cos \varphi_n \end{cases} \quad (3)$$

and

$$\begin{cases} t_1 = t_a \sin \theta_n + t_b \cos \theta_n \\ t_2 = t_b \sin \theta_n - t_a \cos \theta_n \end{cases} \quad (4)$$

$$\begin{cases} t_a = \sin \varphi_L \sin \theta_L \\ t_b = \sin \varphi_L \cos \theta_L \\ t_c = \cos \varphi_L \end{cases} \quad (5)$$

The specular component is expressed as:

$$I_s = D \exp\left(-((E - \theta) / F)^2\right), \quad (6)$$

where  $D = K_s$ ,  $F = \sqrt{2}\sigma$ . Since a Gaussian curve is used to approximate the specular component in the reflection variation,  $E$  is a parameter that indicates the highlight position in the variation curve. In other words, after  $E$  angle rotation, the current point will reach its maximum intensity. The light source direction was fixed and measured in advance, so after we computed the parameters in Eqs. (2) and (6) we were ready to calculate the reflection parameters and surface normal. From Eqs. (3) and (4), the normal is computed as:

$$\begin{cases} \theta_n = \tan^{-1}\left(\frac{(t_b + A t_a / B)}{(A t_b / B - t_a)}\right) \\ \varphi_n = \tan^{-1}\left(\frac{(A + B) t_c}{(C(t_1 + t_2))}\right) \end{cases} \quad (7)$$

The diffuse reflection parameter is given by:

$$K_d = (A t_2 + B t_1) / (2 t_1 t_2 \sin \varphi_n) \quad (8)$$

In the general case, the light source direction vector, view direction vector, and normal vector of a 3D point are not coplanar, so the exponential part in Eq. (6) cannot reach 1.0. Therefore, the estimated parameter  $D$  is not the real specular parameter  $K_s$ . However, we know that when the object is rotated  $E$  degrees, the specular component will reach its maximum. If the angle

between the bisector and normal is  $\beta$ , the specular reflectance can be approximately compensated by:

$$K_s = D / \exp(-(\beta / F)^2), \quad (9)$$

We carried out the computation for each channel. Since six parameters are unknown in Eqs. (2) and (6), mathematically we need at least six samples from six different frames to fit the intensity variation.

### 3.2. Parameter fitting

To estimate each parameter in Eqs. (2) and (6) for each channel, our technique minimizes the sum of the squared intensity errors over all corresponding pixels of each view given by:

$$Err = \sum_k (I(\theta_k; A, B, C, D, E, F) - I_k)^2 = \sum_k e_k \quad (10)$$

This nonlinear minimization problem is solved in our implementation by applying the Levenberg Marquardt iterative method [13].

Unfortunately, this nonlinear iterative method only finds the locally optimal solution. This means that the minimization needs a good initial guess for each parameter. A bad initial guess may prevent the algorithm converging to the expected solution. In our implementation, we made the initial guess for each parameter according to the following method. The initial  $D$  value was the peak value in the measured data for each 3D point. The initial  $E$  value was the position of the peak. The initial  $F$  value was empirically given between 0.01 and 1.0. (We used 0.08 as the initial  $F$  value in our implementation.) Parameters  $A$ ,  $B$ , and  $C$  were given the same initial value. Since the initial values of parameter  $D$  for three channels were already given and could be regarded as a vector in the RGB space, we found the vector from the measured data that had the largest angle with  $D$  in the RGB space. The vector found was used as the initial value of the parameters related to the diffuse component. This method is similar to the method in [9] for computing the body color vector, since the peaks for three channels is considered to be approximate to the light source color vector. However, the difference is that we do not fix the body color vector and light source color vector. These vectors were refined in the algorithm, because the initial guesses for them were not accurate enough, possibly because of noise, measurement error and environment light,

or some other problem.

### 3.3. Separating the two components

When the parameters in Eqs. (2) and (6) have been estimated, the reflectance properties and surface normal can be computed using Eqs. (7), (8), and (9). We get three solutions for the surface normal from the three channels. Since the surface normal is invariant for each channel, these solutions are averaged to obtain the final normal. The mean of the Gaussian distribution and the standard deviation of the facet slope of a 3D point are intrinsic. Therefore, we also compute their average values from the solutions from the three channels. Using the estimated parameter values, the diffuse and specular reflection components  $I'_d$  and  $I'_s$  are computed by applying Eqs. (2) and (6). The separated diffuse and specular components of the original reflectance are then

$$I_d = I * \frac{I'_d}{I'_d + I'_s} \quad I_s = I * \frac{I'_s}{I'_d + I'_s} \quad (11)$$

Since the two components from the model may differ from the original data, we use the results of Eq (11) as the separated diffuse and specular reflection components. Since the sampled intensity variation data contains noise, for a small part of each 3D point, the fitting may result in negative diffuse or specular components. These failure points are interpolated using the separated values of neighboring points.

Note that we use the measured light source direction only to compute the reflectance properties and the normal. We do not need the light source direction and the light source color vector for parameter fitting and separation.

### 3.4. Summary of algorithm

To summarize, our algorithm for estimating the reflectance properties and object shape uses the original reflection data to separate the diffuse and specular reflection components data. The inputs are the color data taken from a surface point with the corresponding pixel in the image sequence and the light direction. The outputs are the reflectance properties, object shape, and separated diffuse and specular reflection components.

The algorithm loops through the following steps

over each surface point:

- ① Compute an initial guess for each fitting parameter in Eqs. (2) and (6);
- ② Estimate the optimal parameters for minimizing the fitting error (10);
- ③ Compute the reflectance properties and surface normal;
- ④ Calculate the reflection components using the estimated parameters.

The advantage of using the Levenberg Marquardt method rather than the straightforward gradient descent is that it converges after fewer iterations.

#### 4. Experimental Results

With the experimental setup shown in Fig. 1, we performed experiments using synthesized and real data obtained from the image sequence. To verify the effectiveness of our algorithm for estimating reflectance properties, we synthesized a group of data using a mechanism similar to the experimental setup. The simulation results are shown in Table 1 where  $K_{dr}$ ,  $K_{dg}$ ,  $K_{db}$  and  $K_{sr}$ ,  $K_{sg}$ ,  $K_{sb}$  are the respective diffuse and specular reflection parameters in the RGB channels. The other parameters were as shown in Fig.2 or as explained in Section 3.

Table 1. Simulation result

	Parameter values used for synthesis	Estimated parameter values
$K_{dr}$	0.777543	0.7775430
$K_{dg}$	0.392522	0.3925219
$K_{db}$	0.491277	0.4912774
$K_{sr}$	0.498124	0.4981243
$K_{sg}$	0.586319	0.5863187
$K_{sb}$	0.638829	0.6388292
$\theta_L$	35.000000°	
$\phi_L$	85.000000°	
$\theta_n$	10.000000°	10.034438°
$\phi_n$	90.000000°	90.000583°
$\sigma$	0.050000	0.0500175

To separate the diffuse and specular reflection components from the intensity variation data of one 3D point (Fig. 3(a)), we initialized the parameters from Eqs. (2) and (6) for the RGB channels. First, we located the peak position, which was at 0.13090 radians (7.5 degrees). The peak values at this position (231.15601, 164.44566, and 192.27081) were given to parameter  $D$  for the three channels. The RGB vector (142.37891, 71.87617, and 89.96966) at 57 degrees provided the initial values of parameter  $A$  for the three channels, because in the RGB color space this vector has the largest angle with the vector formed by parameter  $D$  for three channels [9]. Parameters  $B$  and  $C$  were processed in the same way as  $A$ . Although the standard deviation of the facet slope was 0.05 for the synthesis, 0.08 was used as the initial value in our algorithm. The estimated normalized values were very close to the synthesis values (Table 1). The curves of the synthesized data for each channel are shown in Fig. 3(a). The curves of the two components separated using our algorithm are shown in Fig. 3(b).

In the experiment with real data, we used an HDTV camera (SONY HDC 750A) to obtain a sequence of images of a vase with a complex surface texture. The camera and light source were fixed while the 3D object rotated around the rotation axis (Fig. 1). The camera and rotation axis were well calibrated through a flexible technique [11] for sampling the intensity variation of each 3D point on the object surface. The image resolution was 1920 x 1080 pixels. Our algorithm was implemented through an Onyx2 system with four R10000 processors. The RGB intensity variation for all surface points was produced by a modeling method [14] using 180 frames taken from around the object to model all 3D points on the surface. Although six samples were enough to compute the curve parameters for each 3D point on each channel we took sample data from 31 frames at 4 degrees intervals to form an over-determined nonlinear system. The temporal cost of this algorithm depends on the number of 3D points  $n$ , which is given as  $O(n)$ . The spatial cost is also related to  $n$ , given as  $O(n)$ .

Figure 4(a) shows an image from the image sequence. The reflectance parameters were estimated and then the two components were separated. Figures 4 (b) and (c) show, respectively,

the separated diffuse and specular components. Note that a small part of the vase texture remained in the specular component. This was caused by misregistration between images during

sampling of the pixel intensity variation. A visual comparison with the results given in Nayar et al. [4] shows that our separation was more complete. The experimental results with both synthesized

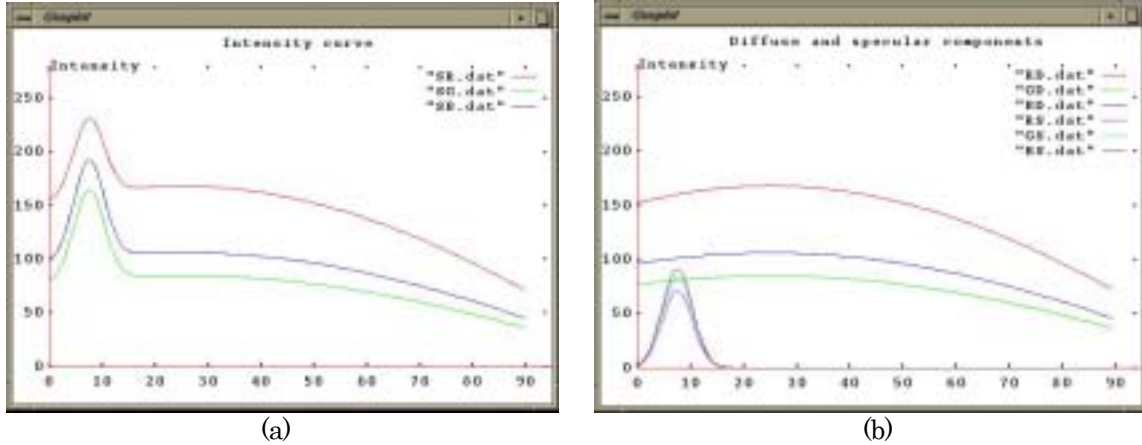


Figure 3. Synthesized RGB data (a) and separated two components (b)

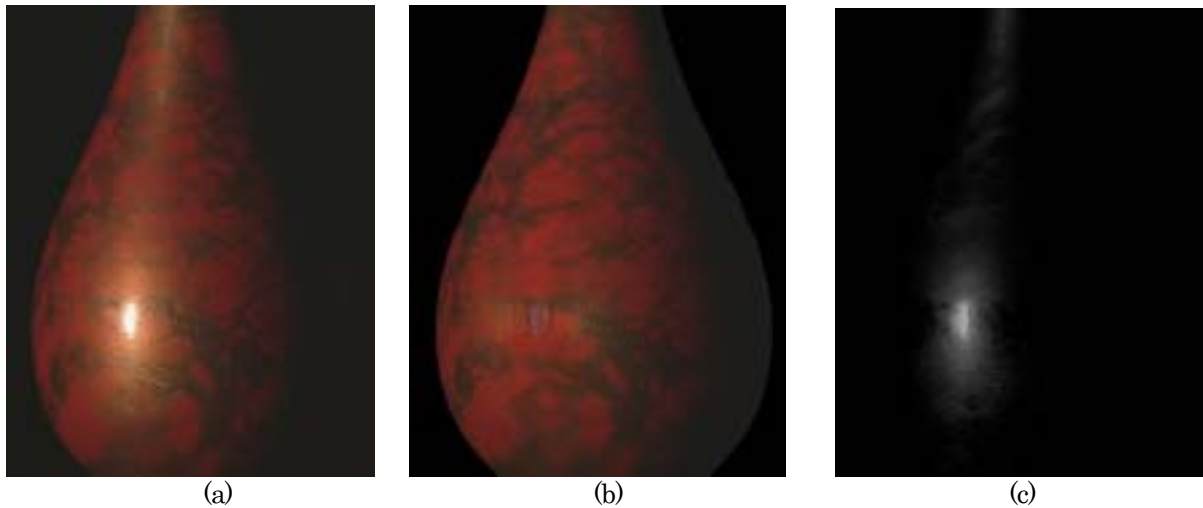


Figure 4. Original image (a); separated diffuse component (b) and specular component (c).

and real data demonstrate the effectiveness of our algorithm.

### 5. Conclusion

We have developed a technique for estimating reflectance properties by observing an actual object and separating the diffuse reflection and specular reflection components using data from images of the actual object. A key feature of our technique is that we estimate the reflectance properties before separation to eliminate the error produced during separation. Another feature is that we estimate both diffuse and specular

parameters at the same time without knowing the body color and light source color, which makes our method more effective and stable. This technique can be used for objects with a complicated texture and high specular reflectance. In principle, it can be applied to complicated object shapes such as shapes with occlusions, if sampled intensity data can be obtained. We will investigate the practicality of this in our future work. We also found that a small area corresponding to the highlight in the diffuse component did not look so natural because of the camera's dynamic range. At present, our

algorithm can only be used for an environment with a single point light source. In our future work, we will experiment with other object shapes and the multi-light source and area light sources.

### Acknowledgement

This work is part of a project supported by TAO.

### REFERENCES

- 1) G. J. Klinker, S. A. Shafer and T. Kanade, "Using a color reflection model to separate highlights from object color", *International Conference on Computer Vision*, pp. 145-150, 1987.
- 2) G. J. Klinker, S. A. Shafer, and T. Kanade, "The measurement of highlight in color images", *International Journal of Computer Vision (IJCV)*, Vol. 2, No. 1, pp. 7-32, 1988.
- 3) G. J. Klinker, S. A. Shafer, and T. Kanade, "A physical approach to color image understanding", *International Journal of Computer Vision (IJCV)*, Vol. 4, No. 1 pp. 7-38, 1990.
- 4) S. K. Nayar, X. S. Fang, and T. Boult, "Separation of reflection components using color and polarization", *International Journal of Computer Vision (IJCV)*, Vol. 21, No. 3, pp. 163-186, 1997.
- 5) K. Ikeuchi and B. K. P. Horn, "Numerical shape from shading and occluding boundaries", *Artificial Intelligence*, Vol. 17, pp. 141-184, August 1981.
- 6) A. P. Pentland, "Local shading analysis", *IEEE Transactions on Pattern Analysis and Machine Intelligence*, Vol. PAMI-6, No. 2, pp. 170-187, March 1984.
- 7) K. Schluns, O. Wittig, "Photometric stereo for non-Lambertian surfaces using color information", *Proceedings of 7<sup>th</sup> International Conference on Image Analysis and Processing*, pp. 505-512, 1993.
- 8) R. J. Woodham, Y. Iwahori, and R. A. Barman, "Photometric stereo: Lambertian reflectance and light sources with unknown direction and strength", Technical Report 91-18, August 1991.
- 9) Y. Sato and K. Ikeuchi, "Temporal-color space analysis of reflection", *Journal of Optical Society of America A*, Vol. 11, No. 11, pp. 2990-3002, November 1994.
- 10) Y. Sato, M. D. Wheeler and K. Ikeuchi, "Object shape and reflectance modeling from observation", *SIGGRAPH'97*, pp. 379-387, 1997.
- 11) Z. Zhang, "A flexible new technique for camera calibration", *IEEE Transactions on Pattern Analysis and Machine Intelligence*, Vol. 22, No. 11, pp. 1330-1334, November 2000.
- 12) K. E. Torrance and E. M. Sparrow, "Theory for Off-specular Reflection from Roughened Surfaces", *Journal of the Optical Society of America, (JOSA)*, No. 57, pp. 1105-1114, 1967.
- 13) W. H. Press et al., "Numerical recipes in C: the art of scientific computing", 2<sup>nd</sup> edition, Cambridge University Press, 1992.
- 14) K. Kobayashi, Y. Nakanishi, X. Zhang, M. Tadenuma, H. Mitsumine and S. Saito: "High resolution 3D surface measurement from multiple viewpoint images", *NICOGRAPH 2000*, pp. 143-150, 2000.
- 15) F. Bernardini, I. M. Martin and H. Rushmeier: "High-quality texture reconstruction from multiple scans", *IEEE Transactions On Visualization and Computer Graphics*, 7(4), pp. 318-332, 2001.